




Cite this: *Chem. Commun.*, 2023, 59, 10444

Received 10th July 2023,  
Accepted 2nd August 2023

DOI: 10.1039/d3cc03294a

rsc.li/chemcomm

# Copper nanoparticle-embellished Zr-based metal–organic framework for electrocatalytic hydrogen evolution reaction†

Ravari Kandy Aparna,<sup>a</sup> Arun Karmakar,<sup>b</sup> Rathnam Tharayil Arsha,<sup>a</sup>  
Subrata Kundu<sup>b</sup> and Sukhendu Mandal<sup>b</sup>  <sup>✉</sup>

**Copper nanoparticles (Cu NPs) have gained immense popularity in catalysis by virtue of their impressive properties and earth abundance. Herein, we incorporated small-sized copper nanoparticles into the amine-functionalized NU-1000 MOF and used this composite material as an effective catalyst for electrocatalytic Hydrogen Evolution Reaction (HER) studies.**

Copper nanoparticles have garnered significant attention in recent years owing to their impressive physical and chemical properties.<sup>1–3</sup> Copper, being the 8th most abundant element on the earth's crust, is inexpensive, and this makes it a cost-effective candidate for applications in various fields such as electronics, machinery, engineering, pharmaceutical, agriculture, energy, environment, *etc.* among which catalysis has gained great recognition because of its versatility and affordability.<sup>3–6</sup> However, the use of copper nanoparticles is often hindered by their inherent instability under atmospheric conditions due to the low redox potential, thus leading to their aggregation. The prevention of agglomeration of Cu NPs is paramount in sustaining the high performance of the catalyst. So, to overcome this, several approaches were used, and among these, anchoring the NPs into porous structures, such as metal–organic frameworks, constitutes a powerful strategy to increase the stability and size tunability of Cu NPs.<sup>7</sup>

Metal–organic frameworks (MOFs) are porous substances with exceptional structural stability<sup>8–10</sup> and these are recognized as excellent supports for NPs. When it comes to catalysis, MOFs hold the upper hand over most of the other porous materials because of their high synthetic tunability, excellent stability, and the potential to provide pore channels for the transmission

of reactants/products.<sup>7,11</sup> Zr-based MOFs are considered perfect candidates as support materials due to their easy synthetic procedure and extraordinary thermal and chemical stability. NU-1000, a Zr-based MOF, is composed of eight connected  $Zr_6(\mu_3-O)_4(\mu_3-OH)_4(H_2O)_4(OH)_4$  nodes at each vertex and tetra-topic 1,3,6,8-*p*-benzoate pyrene (TBAPy<sup>4–</sup>) linkers at each edge.<sup>12</sup> The strong interaction between the carboxylates of the linker and zirconium nodes contributes to the exceptional thermal and chemical stability of NU-1000. The eight terminal non-bridging –OH groups offer great possibility for chemical modifications.<sup>13</sup>

Electrocatalytic water splitting has gained attention as it constitutes a promising strategy for producing hydrogen, which is considered a clean and sustainable fuel.<sup>14</sup> Hydrogen can not only substitute fossil fuels which cause numerous environmental issues but also produce water as the sole product when it is burned with oxygen. The development of a cost-effective, highly efficient catalyst is of paramount importance when it comes to the electrocatalytic hydrogen evolution reaction (HER). Pt-based catalysts are considered to be excellent for HER, but the low earth abundance and high cost of Pt hinder their application. Even though researchers have made significant progress in developing cost-effective electrocatalysts using elements such as Fe, Ni, Co, *etc.*, copper is still much less-explored.<sup>15–17</sup>

In this project, small-sized copper nanoparticles are embedded in NU-1000 MOF, and this NP-MOF composite material is used as a catalyst for electrocatalytic HER. In order to have a better interaction between MOF and Cu NPs, the MOF was functionalized with amine group using a post-synthetic functionalization method, SALI (Solvent assisted ligand incorporation).<sup>13</sup>

A solvothermal procedure was adopted for the synthesis of NU-1000, and the amine functionalization was carried out using the SALI technique with 4-Aminobenzoic acid (4-ABA). The incorporation of Cu NPs has been executed using the solution impregnation method (Scheme 1), which is evidenced by a color change from yellow to brownish-yellow of the material (Fig. S1, ESI†).

<sup>a</sup> School of Chemistry, Indian Institute of Science Education and Research Thiruvananthapuram, Thiruvananthapuram, Kerala-695551, India.

E-mail: sukhendu@iiseriitvm.ac.in

<sup>b</sup> Electrochemical Process Engineering (EPE) Division, CSIR-Central Electrochemical Research Institute (CECRI), Karaikudi-630006, Tamil Nadu, India

† Electronic supplementary information (ESI) available. See DOI: <https://doi.org/10.1039/d3cc03294a>



Powder X-ray diffraction (PXRD) patterns were analyzed for NU-1000 based samples, and the diffraction peaks of NU-1000, NU-1000-NH<sub>2</sub>, and Cu@NU-1000-NH<sub>2</sub> coincide with the peaks of simulated NU-1000 (Fig. S2, ESI†). This confirms that the stability of the parent metal–organic framework is unaltered even after the incorporation of both the amine group and copper nanoparticles. Expected diffraction peaks of metallic copper at 43.4° and 50.6° arising from the planes (110) and (200), respectively, are absent in Cu@NU-1000-NH<sub>2</sub>. This might be due to the small size and low loading of copper nanoparticles. The unchanged rod-like morphology of the framework upon the functionalization, revealed by the SEM images, further corroborates the structural stability of the MOF (Fig. S3, ESI†). In the Fourier Transform Infrared (FTIR) spectroscopy data a shoulder band of primary amine, seen at 3226.9 cm<sup>-1</sup> in case of 4-ABA can also be visualized at 3224.9 cm<sup>-1</sup> in the spectrum of NU-1000-NH<sub>2</sub>, which is absent in NU-1000 (Fig. S4, ESI†). This confirms the incorporation of the -NH<sub>2</sub> into the framework. The slight enhancement of visible light absorption in the case of NU-1000-NH<sub>2</sub> compared to NU-1000 in the UV-DRS spectra of the materials further confirms the presence of the amine group in the functionalized MOF (Fig. S5, ESI†). The peak around 550 nm, corresponding to the surface plasmon resonance peak of Cu NPs in the spectrum of NP@MOF composite validates the incorporation of Cu.<sup>18</sup> The Cu-loading was found to be 12.13 ppm using Inductively coupled plasma-mass spectrometric (ICP-MS) analysis.

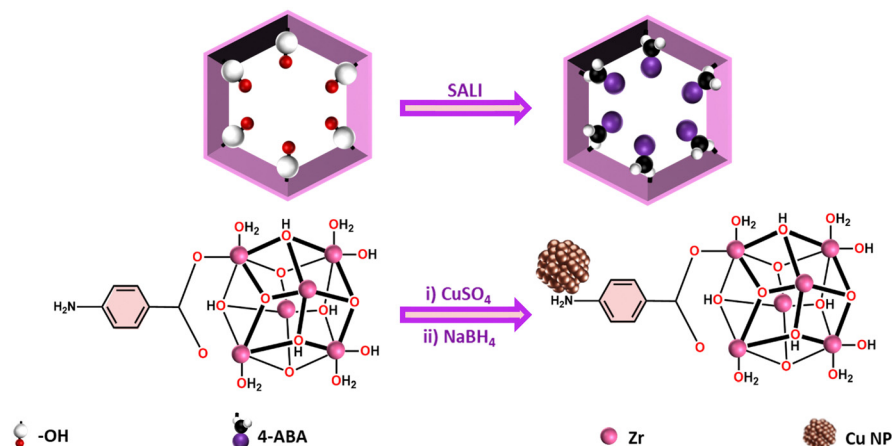
Transmission electron microscopic (TEM) analysis revealed the small size and homogenous distribution of the nanoparticles (Fig. 1a–d). The average size of the nanoparticles was found to be 3.83 ± 0.91 nm. The lattice fringes with a spacing of 0.20 nm, which corresponds to the (111) plane of metallic copper, revealed the high crystallinity of NPs.<sup>19</sup> The elemental mapping using TEM-EDS analysis showed the presence of all the desired elements (Fig. S6, ESI†). This was also supported by SEM-EDS analysis (Fig. S7, ESI†). Brunauer–Emmett–Teller (BET) surface area of NU-1000-NH<sub>2</sub> and Cu@NH-1000-NH<sub>2</sub> were found to be 947.6 m<sup>2</sup> g<sup>-1</sup> to 438.6 m<sup>2</sup> g<sup>-1</sup>, respectively (Fig. S8, ESI†). The reduction of surface area and pore volume after nanoparticle

incorporation might be due to the surface block of the cavities by the incorporated nanoparticles.<sup>20</sup>

The X-ray photoelectron spectroscopic (XPS) survey spectra of NU-1000-NH<sub>2</sub> and Cu@NU-1000-NH<sub>2</sub> show the presence of all the expected elements in the framework (Fig. 1e). Cu 2p spectrum shows two spin-orbit components at 932.8 eV and 952.6 eV (for Cu 2p<sub>3/2</sub> and 2p<sub>1/2</sub>, respectively). The oxidation state of Cu could be zero as satellite peaks are absent in the spectrum (Fig. 1f).<sup>22</sup> N 1s spectrum of NU-1000-NH<sub>2</sub> has binding energy at 399.7 eV, which confirms the presence of primary amine in the material.<sup>21</sup> There is a decrease in the binding energy of N 1s spectrum to 399.2 eV after the incorporation of copper nanoparticles in NU-1000-NH<sub>2</sub> (Fig. 1g and h). This validates the electronic interaction between the amine group and the introduced copper nanoparticles.

Initial activity towards HER is primarily monitored by linear sweep voltammetry (LSV) in 0.5 M H<sub>2</sub>SO<sub>4</sub> solution (pH = 0.3) with a lower scan rate of value of 5 mV s<sup>-1</sup>. From Fig. 2a, it is notable that initial polarization towards HER started at a lower applied potential region as compared to pristine MOF. The Cu@NU-1000-NH<sub>2</sub> portrays a lower overpotential value of 158 mV to drive 10 mA cm<sup>-2</sup> current density value, while the pristine MOF demands a higher potential value of 615 mV to drive the same current density. Meanwhile, the Cu@ NU-1000-NH<sub>2</sub> delivers a much higher magnitude of HER current density than the pristine MOF (Fig. 2b). The charge transfer kinetics at the electrode–electrolyte interface for both materials have been analyzed from the Tafel plot acquired from the iR-drop free LSV information (Fig. 2c). The Cu@NU-1000-NH<sub>2</sub> possesses a lower Tafel slope value of 105 mV dec<sup>-1</sup>, whereas the calculated Tafel slope value was 392 mV dec<sup>-1</sup> for pristine MOF. The lower Tafel slope value for Cu@NU-1000-NH<sub>2</sub> indicates a faster charge transfer kinetics with electrochemical desorption (Volmer–Heyrovsky step) as the RDS of the H<sub>2</sub> molecule at the interface.

Charge transfer resistance (*R*<sub>ct</sub>) towards the electron transfer at the interface was calculated by EIS analysis, and obtained EIS features have been portrayed in Fig. 3a. The calculated *R*<sub>ct</sub> values were 6.35 and 37.79 Ω for Cu@NU-1000-NH<sub>2</sub> and pristine MOF, respectively. To verify the high HER capability of



Scheme 1 Schematic diagram of the synthesis of Cu@NU-1000-NH<sub>2</sub>.



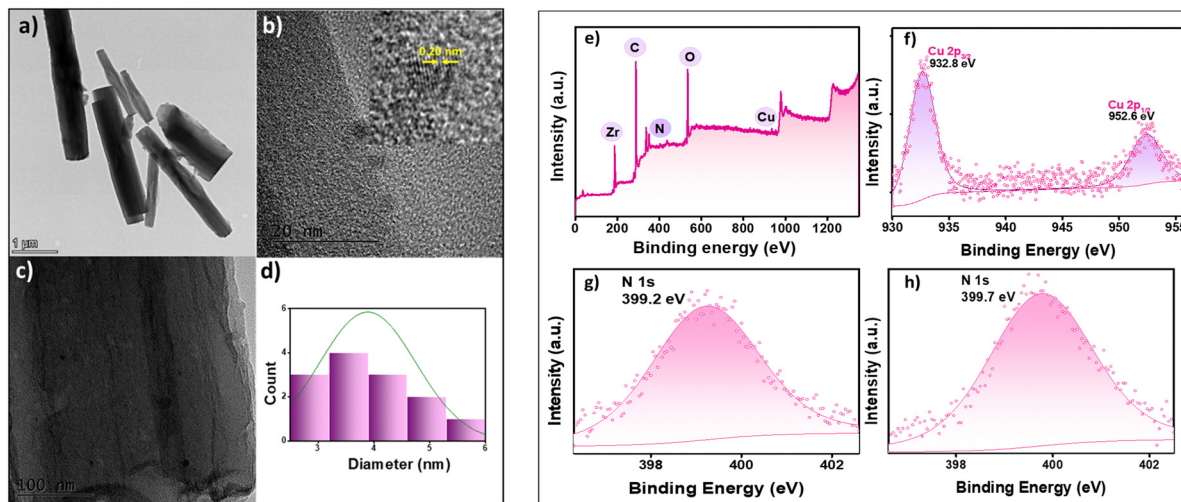


Fig. 1 (a)–(c) HR-TEM images, (d) size distribution histogram of Cu@NU-1000-NH<sub>2</sub>, (e) XPS survey spectrum, (f) spectrum of Cu 2p, (g) spectrum of N 1s of Cu@NU-1000-NH<sub>2</sub> and (h) spectrum of N 1s of NU-1000-NH<sub>2</sub>.

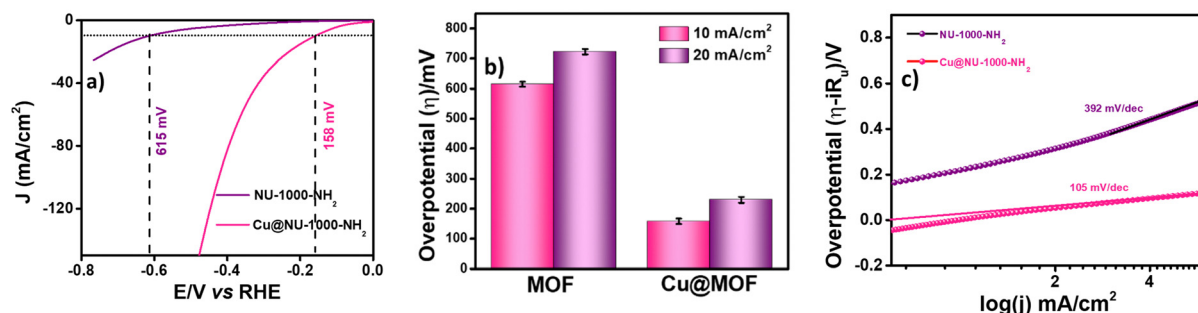


Fig. 2 HER performance of the catalysts. (a) LSV curves, (b) bar diagram representing the over potential at 10 mA cm<sup>-2</sup>, (c) Tafel slopes of NU-1000-NH<sub>2</sub> and Cu@NU-1000-NH<sub>2</sub>.

Cu@NU-1000-NH<sub>2</sub>, the analysis of exposed active sites by double layer capacitance ( $C_{dl}$ ) method was carried out.

The scan rate-dependent CV curves have been portrayed in Fig. S9 (ESI<sup>†</sup>) for both Cu@NU-1000-NH<sub>2</sub> and pristine MOF, respectively. From the slope of the given  $J$  vs. scan rate plot (Fig. 3b), the  $C_{dl}$  values for Cu@NU-1000-NH<sub>2</sub> and pristine MOF are 2.35 and 0.74 mF cm<sup>-2</sup>, respectively. The TOF value of Cu@NU-1000-NH<sub>2</sub> is calculated to be 1.97 s<sup>-1</sup> (see ESI<sup>†</sup> for calculation). The durability of the catalyst was verified *via* chronoamperometric (CA) study for 45 hours with a constant applied potential of -0.3 V vs. RHE. The resulting CA outcome is portrayed in Fig. 3c. The amount of hydrogen formed was monitored using GC-MS analysis by measuring the produced gas under the application of a constant potential. According to Faraday's second law of electrolysis, the amount of produced gas has been compared with the calculated amount, and faradaic efficiency was found to be 91.55% (Fig. S10, ESI<sup>†</sup>).

This as-synthesized catalyst showed impressive catalytic activity and stability compared to other Cu-based catalysts (Table S1, ESI<sup>†</sup>).

Post-catalytic stability of the catalyst was investigated using various techniques. HR-TEM analysis shows the rod-like

morphology of the MOF was retained, and the presence of all the expected elements, including Zr, N, and Cu, were confirmed using TEM-EDS elemental mapping (Fig. S11c–f, ESI<sup>†</sup>). PXRD plot of the catalyst coated on carbon cloth after the catalysis revealed that the peaks remained unchanged. This depicts the persisting crystallinity of the material (Fig. S12, ESI<sup>†</sup>). In order to study the leaching of Cu ion from the catalyst, ICP-MS analysis was done for the electrolyte solution of the chronoamperometric measurement. The amount of copper in the electrolyte was found to be 0.001 ppm which indicates the negligible leaching of the metal. Post-catalytic XPS analysis also corroborates the presence of all the desired elements (Fig. S13, ESI<sup>†</sup>). The binding energy values of Cu 2p<sub>3/2</sub> and 2p<sub>1/2</sub> were found to be 933.7 and 953.1 eV, respectively, which is close to the binding energy values of the pre-catalytic sample. In the case of the N 1s spectrum, the BE values were obtained at 399.5 eV which is also near enough to that of the sample before catalysis.

Copper is a less-explored element for HER, which is considered an efficient strategy for producing hydrogen fuel. Even though copper is earth-abundant and inexpensive, stabilization of monodispersed small Cu nanoparticles is challenging due to their low redox potential in ambient conditions. Here, we



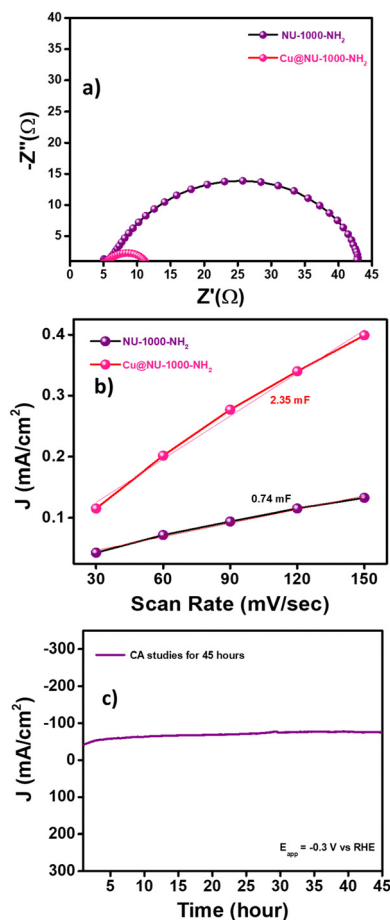


Fig. 3 (a) Nyquist plots, (b) linear fit for estimating the double-layer capacitance of UiO-66-SH and Cu@NU-1000-NH<sub>2</sub> and (c) chronoamperometry measurements for the stability test of Cu@NU-1000-NH<sub>2</sub>.

synthesized monodispersed small sized Cu NPs onto the amine functionalized zirconium-based MOF scaffold. Several state-of-the-art characterizations methods established the composition and structural morphology of this NP-MOF composite material. This composite material delivered an efficient HER activity with an overpotential of 158 mV (current density of 10 mA cm<sup>-2</sup>) and Tafel slope of 105 mV dec<sup>-1</sup> with cycling stability of 45 h (without any structural change).

RKA, AK, and ART did all the experiments, SM conceived and SK and SM supervised the project, and all the authors contributed to the manuscript write-up.

We acknowledge Science Engineering and Research Board (SERB) (Govt. of India) for the financial support through grant CRG/2022/000984. CECRI manuscript number: CECRI/PESVC/Pubs/2023-098.

## Conflicts of interest

There are no conflicts to declare.

## References

- 1 J. Zhang, J. Liu, Q. Peng, X. Wang and Y. Li, *Chem. Mater.*, 2006, **18**, 867–871.
- 2 A. K. Patra, A. Dutta and A. Bhaumik, *Catal. Commun.*, 2010, **11**, 651–655.
- 3 M. B. Gawande, A. Goswami, F. X. Felpin, T. Asefa, X. Huang, R. Silva, X. Zou, R. Zboril and R. S. Varma, *Chem. Rev.*, 2016, **116**, 3722–3811.
- 4 D. Kim, C. S. Kley, Y. Li and P. Yang, *Proc. Natl. Acad. Sci. U. S. A.*, 2017, **114**, 10560–10565.
- 5 M. C. Crisan, M. Teodora and M. Lucian, *Appl. Sci.*, 2021, **12**, 141.
- 6 M. Bakshi and A. Kumar, *Chemosphere*, 2021, **281**, 130940.
- 7 C. Rösler and R. A. Fischer, *CrystEngComm*, 2015, **17**, 199–217.
- 8 H. Furukawa, K. E. Cordova, M. O'Keeffe and O. M. Yaghi, *Science*, 2013, **341**, 1230444.
- 9 H.-C. Zhou, J. R. Long and O. M. Yaghi, *Chem. Rev.*, 2012, **112**, 673–674.
- 10 M. Safaei, M. M. Foroughi, N. Ebrahimipour, S. Jahani, A. Omid and M. Khatami, *TrAC, Trends Anal. Chem.*, 2019, **118**, 401–425.
- 11 R. K. Aparna, V. Surendran, D. Roy, B. Pathak, M. M. Shaijumon and S. Mandal, *ACS Appl. Energy Mater.*, 2023, **6**, 4072–4078.
- 12 T. Islamoglu, K. I. Otake, P. Li, C. T. Buru, A. W. Peters, I. Akpinar, S. J. Garibay and O. K. Farha, *CrystEngComm*, 2018, **20**, 5913–5918.
- 13 P. Deria, W. Bury, J. T. Hupp and O. K. Farha, *Chem. Commun.*, 2014, **50**, 1965–1968.
- 14 M. G. Walter, E. L. Warren, J. R. McKone, S. W. Boettcher, Q. Mi, E. A. Santori and N. S. Lewis, *Chem. Rev.*, 2010, **110**, 6446–6473.
- 15 R. Mejia-Rodriguez, D. Chong, J. H. Reibenspies, M. P. Soriaga and M. Y. Darensbourg, *J. Am. Chem. Soc.*, 2004, **126**, 12004–12014.
- 16 V. Artero, M. Chavarot-Kerlidou and M. Fontecave, *Angew. Chem., Int. Ed.*, 2011, **50**, 7238–7266.
- 17 O. R. Luca, S. J. Konezny, J. D. Blakemore, D. M. Colosi, S. Saha, G. W. Brudvig, V. S. Batista and R. H. Crabtree, *New J. Chem.*, 2012, **36**, 1149–1152.
- 18 N. L. Pacioni, A. Pardoe, K. L. McGilvray, M. N. Chrétien and J. C. Scaiano, *Photochem. Photobiol. Sci.*, 2010, **9**, 766–774.
- 19 G. Cheng and A. R. Hight Walker, *Anal. Bioanal. Chem.*, 2010, **396**, 1057–1069.
- 20 L. Vradman, M. V. Landau, D. Kantorovich, Y. Koltypin and A. Gedanken, *Microporous Mesoporous Mater.*, 2005, **79**, 307–318.
- 21 L. Shen, W. Wu, R. Liang, R. Lin and L. Wu, *Nanoscale*, 2013, **5**, 9374–9382.
- 22 M. Raja, J. Subha, F. B. Ali and S. H. Ryu, *Mater. Manuf. Processes*, 2008, **23**, 782–785.

